

# A Local Appearance Model for Volumetric Capture of Diverse Hairstyles

Ziyan Wang<sup>1,2</sup> Giljoo Nam<sup>2</sup> Aljaz Bozic<sup>2</sup> Chen Cao<sup>2</sup>  
 Jason Saragih<sup>2</sup> Michael Zollhöfer<sup>2</sup> Jessica Hodgins<sup>1</sup>

<sup>1</sup>Carnegie Mellon University <sup>2</sup>Reality Labs Research

## Abstract

*Hair plays a significant role in personal identity and appearance, making it an essential component of high-quality, photorealistic avatars. Existing approaches either focus on modeling the facial region only or rely on personalized models, limiting their generalizability and scalability. In this paper, we present a novel method for creating high-fidelity avatars with diverse hairstyles. Our method leverages the local similarity across different hairstyles and learns a universal hair appearance prior from multi-view captures of hundreds of people. This prior model takes 3D-aligned features as input and generates dense radiance fields conditioned on a sparse point cloud with color. As our model splits different hairstyles into local primitives and builds prior at that level, it is capable of handling various hair topologies. Through experiments, we demonstrate that our model captures a diverse range of hairstyles and generalizes well to challenging new hairstyles. Empirical results show that our method improves the state-of-the-art approaches in capturing and generating photorealistic, personalized avatars with complete hair.*

## 1. Introduction

Creating and capturing high-fidelity 3D human avatars is an essential capability for mixed reality. A high-quality, photorealistic 3D avatar can blur the boundary between the real and virtual world and facilitate VR/AR applications such as social telepresence, virtual gaming and virtual shopping. One critical aspect of achieving a lifelike avatar is accurately capturing and modeling hair, as it plays a vital role in establishing personal identity and achieving personalized avatars. However, hair is potentially challenging to capture due to its complex geometry and high-frequency texture. Furthermore, different hairstyles exhibit large intra-class variance in terms of appearance and shape, which adds to the complexity of efficiently creating personalized avatars for a large group of individuals.

In this work, we look at the problem of how to capture diverse hair appearance for efficient and accurate creation

of photorealistic, personalized 3D avatars. Given the complexity of hair geometry, several 3D representations have been explored with the goal of improving modeling accuracy. Mesh-based representations work well for capturing the surface details and are most efficient to store. But they are not well-suited for modeling hairstyles that exhibit volumetric properties. Strand-based representations can capture hair with the highest accuracy and are easy to manipulate. However, modeling and rendering complex hairstyles with strand-based representations can be computationally expensive. In comparison, many recent volumetric-based methods [9–11, 14, 15, 33, 34, 45, 54, 56] modeled human avatars with photorealistic hairstyles with diverse geometry and appearance. The avatars can be optimized from images or videos via differentiable raymarching in an end-to-end learning framework. However, the model accuracy relies on a person-specific model which does not generalize and requires extensive training time. Those properties prohibit these approaches from creating personalized avatars for a large group of individuals.

To achieve both efficiency and accuracy in creating personalized avatars for individuals, we present a universal 3D hair appearance model that captures diverse hairstyles with high fidelity and helps to generate high-quality hair appearance for personalized avatar creation. Our universal 3D hair appearance model is conditioned on a group of hair feature volumes that are diffused from a 3D hair point cloud with color. Those hair feature volumes are anchored by volumetric primitives that tightly bound the hair point cloud, and reflect the local structures and appearance at a primitive level. To amplify the sparse point cloud for dense appearance modeling, we learn a UNet to transfer those hair feature volumes into dense radiance fields. By spatially compositing those volumetric primitives, we get a set of volumetric radiance fields that fully cover different parts of the hair. Those volumetric radiance fields are not restricted to certain topologies and can model different hairstyles. The design choice to learn an appearance prior at a primitive level rather than the hairstyle level is based on the observation that different hairstyles share a more similar pattern within a local region than at a global scale. Learning a com-

pact embedding space at a global scale to express such variety is nearly implausible, with a limited amount of training data. Learning a local prior model helps us to achieve better generalization as it splits each hairstyle into multiple local volumetric primitives.

We conduct extensive experiments on multiview captures of multiple identities as well as in-the-wild captures of new identities with a limited number of viewpoints. We empirically show that our method outperforms previous state-of-the-art methods [4, 26] in capturing diverse hairstyles, demonstrating improved quality and generalizing to new hairstyles for personalized avatar creation. Given sparse views as input, we also find that our local prior model serves as a good initialization for more efficient acquisition of personalized avatars with less finetuning. In summary, our contributions are

- We present a novel volumetric feature representation based on a point cloud with color and a local appearance model that is generalizable to various complex hairstyles.
- We empirically show that our method outperforms previous state-of-the-art approaches in capturing high-fidelity avatars with diverse hairstyles and generating photorealistic appearances for novel identities with challenging hairstyles. Our method also enables the efficient capture of personalized avatars from an iPhone captures.

## 2. Related Works

In this section, we will discuss related literature on hair modeling, neural radiance fields and volumetric avatars.

### 2.1. Hair Strand Reconstruction

Multiview stereo has been heavily explored in reconstructing hair strand representation from visual capture systems. Early works [31, 32, 47] utilize 2D orientation maps as additional information for doing triangulation on 3D strand structures. Luo *et al.* [24, 25] and Hu *et al.* [12] fit structural hair representations like strands and ribbons into point cloud from MVS for hair reconstruction. Nam *et al.* [29] relax the plane assumption in PatchMatch MVS for thin strand reconstruction and Sun *et al.* [41] leverages patterned illuminations for high-fidelity strand geometry as well as reflectance material recovery. NeuralStrands [39] learns a neural hair generator for hair structure fitting from the reconstruction. NeuralHDDHair [48] and DeepMVSHair [16] learn to regress a hair growing field for hair strand generation based on sparse multiview images of hair. However, those methods require a dense camera array and long optimization time which is prohibitive for creating avatars to individuals. Compared to the hair capture methods using a multiview capture system, many works [5, 6, 13, 18, 40, 49, 53, 55, 57] explore hair reconstruction from a single view which is easier to scale up. They take advantage of the existing database of synthetic

3D hair or user interactions to serve as a prior for inferring the underlying hair structure given partial observation like a monocular video or image. However, those methods usually generate overly smooth results and are limited in resolution. Furthermore, they are also limited by the variety of the existing synthetic hair datasets, which hampers their models’ ability to generate complex hairstyles like hair bundles or extremely curly hair.

### 2.2. Neural Radiance Fields

Neural radiance fields (NeRF) [27] learn a radiance field from multiple calibrated RGB images via differentiable volumetric raymarching, where they parameterize the radiance field implicitly with MLPs. As a result of its simplicity and impressive results, many recent works have improved NeRF on dimensions such as accurate geometry [30, 43, 50] and anti-aliasing [1–3]. However, most of these approaches suffer from long training times and are not very efficient to render.

Many works [20, 21, 28, 37, 51] have focused on improving the rendering efficiency of NeRF. AutoInt [20] speeds up the volumetric raymarching process by learning closed-form solutions to the integral in volumetric raymarching. NSVF [21] and PlenOctrees [51] both optimize the run-time efficiency of NeRF by stacking it in a sparse structure like an octree. KiloNeRF [37] optimizes the run-time efficiency by shortening the model inference time by substituting a single MLP with multiple tiny and shallow MLPs. TensRF [8] factorizes the 4D tensor of radiance field into compact components like vector and matrix which leads to not only smaller model size but also more efficient reconstruction of the scene. Instant-NGP [28] combines both tiny MLP and sparse structures. Furthermore, to achieve efficient storage of the radiance field without losing the reconstruction fidelity, a spatial hash function is presented to store the multi-resolution spatial features which will be used as input to the tiny MLP to retrieve the radiance value. Our method also leverages sparse structures for efficient rendering of radiance fields.

### 2.3. Volumetric Avatar

Most recently, volumetric representation is favored in avatar creation due to its completeness in modeling various hair geometry and its simplicity in optimization via a differentiable volumetric raymarching. Neural Volumes [22] first presents a compact formulation for differentiable volumetric raymarching for creating a volumetric head avatar with photorealistic hair from multiview RGB videos. One of the follow-up works [44] combines the volumetric representation and coordinate-based representation into a hybrid form for better rendering quality and drivability. With the recent success of NeRF [27] in modeling 3D scenes with good appearance from multiple images, there are many works for

building avatar with NeRF [9–11, 14, 15, 26, 33, 34, 36, 54, 56]. Those NeRF-based avatars are typically composed of a spatial 3D warp field and a canonical appearance field. Nerfies [33] learns a volumetric deformation field and canonical space NeRF for modeling dynamics-related changes. HyperNeRF [34] uplifts the deformation field from 3D Euclidean space to a high dimensional hyper semantic space to better model large variations in expressions. NeRFace [9] improves the controllability of NeRF-based avatars by using a 3D face morphable model to control the radiance field defined on faces. IM Avatar [54] improves NeRFace for more complete expressions based on implicit skinning fields following FLAME [17]. HeadNeRF [11] learns a parametric head model with illumination using NeRF. PointAvatar [56] learns a point cloud-based avatar with a temporally conditioned volumetric deformation field for capturing a 3D avatar from video. INSTA [58] builds an efficient pipeline for learning a NeRF-based avatar based on instant-npg [28]. However, those methods mostly assume hair to be rigidly attached to the head without motion. And most of them are still limited by the prohibiting rendering time which is also the limitation of NeRF.

In contrast to the line of NeRF-based avatars, a mixture of volumetric primitives (MVP) [23] builds a volumetric representation that can generate extremely high-quality and real-time renderings that look realistic even on challenging materials, like hair and clothing. The key idea is to model a dynamic head by stacking multiple volumetric primitives only on a tracked head mesh, without wasting memory on empty spaces. Following MVP, HVH [45] models hair and head in separate layers and present a hybrid model of guide hair stands and volumetric primitives. A structure-aware strand tracking algorithm and a 3D scene flow optimization method are presented for dynamic capture of hair. NeuWigs [46] further improves the tracking robustness and builds a data-driven model for hair animation. However, similar to the line of NeRF-based avatars, those methods build a person-specific model which does not generalize to novel identities and it is non-trivial to reuse those methods for large-scale capture of diverse avatars due to the large variance in hair topology and appearance.

Some recent works [4, 26, 36] looked at the problem of building a generalizable model for scalable avatar creation. Pixel-Aligned Avatars [36] utilizes pixel-aligned information as additional inputs for NeRF to extend its drivability and generalization over sequence data. Inspired by PixelNeRF [52] and MVSNeRF [7], KeypointNeRF [26] improves the generalization of avatars and NeRF’s robustness to sparse views by using a new spatial encoding technique with sparse 3D key points. However, they are usually limited to modeling very complex geometry and are restricted to small camera baseline setups. Cao *et al.* [4] extends MVP to in-the-wild scenarios and unseen faces. By learning a

cross-identity hyper network that controls the expression and identity change on volumetric avatars from a large corpus of data, the model can be easily adapted to newly captured identities even from an iPhone scan. However, it relies on an accurately tracked head mesh for recovering the volumetric texture on top of it and is limited to model hairstyles that can not be approximated by a spherical mesh surface.

### 3. Method

Our goal is to achieve efficient and accurate hair appearance capture of a large number of individuals with a single model. We use a compositional volumetric representation for hair modeling. There are several benefits of using such a representation for hair modeling. First, volumetric representation is flexible enough to model complex hair configuration while also yielding a decent rendering quality with high fidelity on detailed geometry. Second, rendering a compositional volumetric representation is more efficient than a volumetric representation, as the raymarching process is guided by a sparse structure to skip empty spaces. To accommodate the diverse topology as well as capture the generalizable prior of various hairstyles, we learn a local hair appearance prior model  $\Psi_\alpha$  and  $\Psi_{rgb}$  that can regress the compositional volumetric presentation based on sparse color point clouds  $q$ . The model takes input as a group of local hair feature volumes diffused by the colored hair point cloud, which is agnostic to the ordering of the point cloud and outputs a compositional volumetric representation  $\mathbf{V}_{rgb} + \mathbf{V}_\alpha$  that can be rendered from different viewpoints.

#### 3.1. Preliminaries: Volumetric Rendering

We render and optimize our compositional volumetric representation with the differentiable volumetric raymarching algorithm in MVP [23]. Given the camera center as  $c$  and a ray direction  $v(p)$  associated with pixel  $p$ , we can define a ray function  $r$  as follow:

$$r(p) = c + \tau v(p),$$

where  $\tau$  is the traversal depth along the ray and  $v(p)$  is the direction starting from camera center  $c$  and pointing to pixel  $p$ .

To render the compositional volumetric representation, we aggregate all the alpha, the RGB values and the semantic labels from the volumetric field. The image formation process can be formulated as:

$$\begin{aligned} \mathcal{I}_p &= \int_{\tau_{min}}^{\tau_{max}} \mathbf{V}_{rgb}(\mathbf{r}_p(\tau)) \frac{dT(\tau)}{d\tau} d\tau, \\ \mathcal{M}_p &= \int_{\tau_{min}}^{\tau_{max}} \mathbf{V}_{label}(\mathbf{r}_p(\tau)) \frac{dT(\tau)}{d\tau} d\tau, \\ T(l) &= \min\left(\int_{\tau_{min}}^{\tau_{max}} \mathbf{V}_\alpha(\mathbf{r}_p(\tau)) d\tau, 1\right), \end{aligned}$$

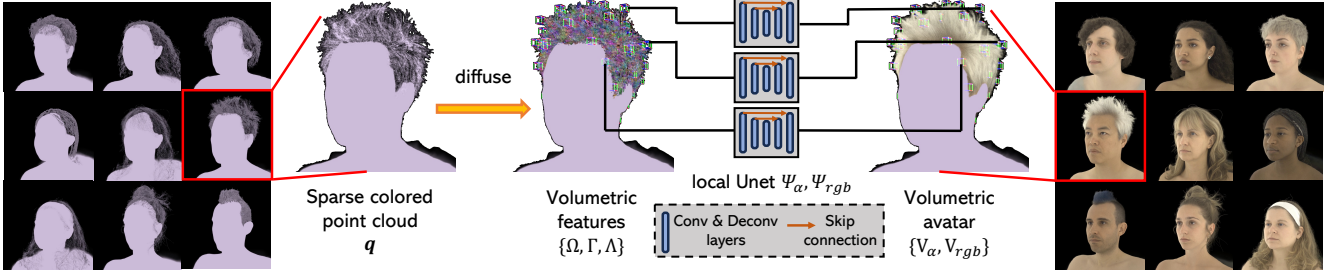


Figure 1. **Pipeline of Our Method.** We present a pipeline to achieve large scale capture of diverse hairstyles for avatar creation. The core of our pipeline is a local UNet that can generate local appearance field conditioned on colored point cloud  $q$ . Our method is robust to various challenging hairstyles and can generate photorealistic appearance of those hairstyles.

where we composite the RGB and semantic label from near to far in a weighted sum manner.  $\mathbf{V}_{\clubsuit}(\cdot)$  indicates the volumetric field function that outputs the function value of a specific spatial point, where  $\clubsuit$  can be alpha, RGB, or a semantic label. For efficient rendering of  $\mathbf{V}_{\clubsuit}$ , we use a BVH to speed up the process of finding intersections between rays and volumetric primitives following MVP [23].

To get the full rendering, we composite the rendered image as  $\tilde{\mathcal{I}}_p = \mathcal{I}_p + (1 - \mathcal{A}_p)I_{p,bg}$  where  $\mathcal{A}_p = T(l_{max})$  and  $I_{p,bg}$  is the background image. Similar to NeuWigs [46], we model the hair and head of an avatar in separate layers and render their segmentation map as  $\mathcal{M}_p$ . Please refer to the supplemental materials for implementation details.

### 3.2. Local Hair Appearance Prior Model

In this part, we describe how we achieve the conditional generation of  $\mathbf{V}_{alpha}$  and  $\mathbf{V}_{rgb}$  based on sparse colored hair point cloud  $q$  with a local appearance prior model. We will first describe how we create the input to the local appearance model with a colored hair point cloud. Then we will introduce our design for the architecture of the local appearance prior model as well as objectives for training the model.

**Hair feature volumes.** As different hairstyles might be in different topologies and different sizes, it is not practical to learn a model that has a fixed output size to regress the appearance field of both long hair and short hair in the 3D space directly. To achieve modeling across different hairstyles and capture the common appearance prior among them, we learn a local appearance prior model to regress the radiance field for each of those hair volumes in separate runs. Given a colored hair point cloud  $q$  defined in a head-centered coordinate system, we prepare the input to the local appearance prior model by first partitioning it into a group of hair feature volumes. Specifically, we first perform furthest point sampling [35] on  $q$  to get  $k$  centroids  $\{\rho_i | i = 1, 2, \dots, k\}$  that roughly span over the point cloud manifold uniformly. Then for each centroid  $\rho_i$ , we diffuse the points into a volume grid  $\Omega^{\rho_i}$  centered at  $\rho_i$ . The vol-

ume grid is axis-aligned with the head-centered coordinate system with a length of  $\delta$  and a grid resolution of  $m$ . Each vertex in the grid  $\Omega^{\rho_i}$  stores both the spatial occupancy and RGB values, where the occupancy is 0 if no point is found within the radius of  $\sqrt{3}\delta/2m$  around that vertex otherwise 1. The RGB value will be the mean of the colors from all found points and 0 if no point is found. In addition to the occupancy and RGB value, we aggregate the spatial coordinate of each vertex in the head-centered coordinates as well as the per-vertex viewing direction into volume grids  $\Gamma^{\rho_i}$  and  $\Lambda^{\rho_i}$  respectively. Given viewing direction camera center  $c$  under the head centered coordinate, we calculate  $\Lambda^{\rho_i} = \text{norm}(\Gamma^{\rho_i} - c)$  where we take the normalized vector between each point in  $\Lambda^{\rho_i}$  and  $c$  as the per-vertex viewing direction.

**Local appearance UNet.** We learn two separate UNets [38] with skip connections that takes volume grid  $\Omega^{\rho_i}$  as input and outputs the corresponding dense radiance field  $\nu_{\alpha}^{\rho_i}$  and  $\nu_{rgb}^{\rho_i}$  respectively as follows:

$$\begin{aligned} \nu_{\alpha}^{\rho_i} &= \Psi_{\alpha}(\Omega_i^{\rho_i}, \Gamma^{\rho_i} | \theta_{\alpha}) \\ \nu_{rgb}^{\rho_i} &= \Psi_{rgb}(\Omega_i^{\rho_i}, \Gamma^{\rho_i}, \hat{c}, \Lambda^{\rho_i} | \theta_{rgb}), \end{aligned}$$

where  $\theta_{\alpha}$  and  $\theta_{rgb}$  are the learnable parameters for each network. By spatially compositing the volumetric primitives  $\{\nu_{\alpha}^{\rho_i}, \nu_{rgb}^{\rho_i} | i = 1, 2, \dots, k\}$  with respect to their centroids  $\{\rho_i | i = 1, 2, \dots, k\}$ , we get  $\mathbf{V}_{alpha}$  and  $\mathbf{V}_{rgb}$ . The UNet  $\Psi_{\alpha}(\cdot)$  that regresses the alpha field of hair takes the occupancy and RGB field  $\Omega^{\rho_i}$  as well as the grid coordinate  $\Gamma^{\rho_i}$  as input. To model the view conditioned appearance of hair, we learn a separate UNet  $\Psi_{rgb}(\cdot)$  to regress the RGB field  $\nu_{rgb}^{\rho_i}$  that takes additional input of the per-vertex viewing direction  $\Lambda^{\rho_i}$  as well as the normalized camera center  $\hat{c}$  as viewing direction.  $\Lambda^{\rho_i}$  is served as additional information to the input of the UNet  $\Psi_{rgb}(\cdot)$  and  $\hat{c}$  is injected at the bottleneck level where it is repeated and appended to every hair features at the coarsest resolution map. We find that the usage of  $\Gamma^{\rho_i}$  and  $\Lambda^{\rho_i}$  improves the model's convergence by a large margin, which will be discussed in detail in the ex-

periment section. The encoder part of each UNet consists of convolutional layers with a kernel size of  $3 \times 3$  with stride 1 and 2 to extract the features of  $\Omega_i^\rho$  at different scales. The decoder part of each UNet consists of convolutional layers with a kernel size of  $3 \times 3$  with stride 1 and deconvolutional layers with a kernel size of  $4 \times 4$  with stride 2. At each scale, we use a  $1 \times 1$  convolutional layer as skip connections to add early conditions from the encoder features to the decoder features respectively. All layers are followed with a LeakyReLU layer as activation. We find that the usage of skip connections can greatly help the network to capture detailed geometry and more salient textures on the regressed hair radiance field.

**Training objectives and details.** To learn the parameters  $\theta_\alpha$  and  $\theta_{rgb}$  of the local appearance model  $\Psi_\alpha(\cdot)$  and  $\Psi_{rgb}(\cdot)$ , we construct image level reconstruction losses. We formulate the training objective  $\mathcal{L}$  as below:

$$\mathcal{L} = \mathcal{L}_1 + \lambda_{VGG} \mathcal{L}_{VGG} + \lambda_{seg} \mathcal{L}_{seg},$$

where  $\lambda_{VGG}$  and  $\lambda_{seg}$  are positive values for rebalancing each term in the training objectives. The first term  $\mathcal{L}_1$  measures the difference between the rendered image  $\tilde{I}$  and the ground truth image  $I_{gt}$ . The second term is a perceptual loss between the rendered image  $\tilde{I}$  and the ground truth image  $I_{gt}$ , which aims at enhancing the visual quality and adding high frequency details of the rendered image. The third term is a segmentation loss for better disentangling hair and non-hair regions. Please refer to the supplemental materials for more training related details.

## 4. Experiments

**Dataset.** We collect a multiview RGB image dataset of multiple identities with diverse personalized hairstyles. The dataset contains lightstage capture of around 260 identities and each capture has around 160 views covering most perspectives around the participant with a focus on the head and hair region. We exclude captures of 8 identities from training our model and use them just for test purposes. For all 256 training identities, we also hold out 7 views for testing and the rest of the views will be used for training.

### 4.1. Novel View Synthesis

We test our model on the task of novel view synthesis and compare it with previous state-of-the-art approaches on generating personalized avatars like the universal prior model(UPM) in Cao *et al.* [4] and a generalizable NeRF model KeypointNeRF [26]. We evaluate different methods using image reconstruction and similarity metrics like MSE, PSRN, SSIM and LPIPS between the ground true image and the reconstructed ones, which are reported in Tab. 1. In the upper part of the table, we report the metrics computed on the holdout views of the training identities. The results in Tab. 1 are supposed to reflect how well

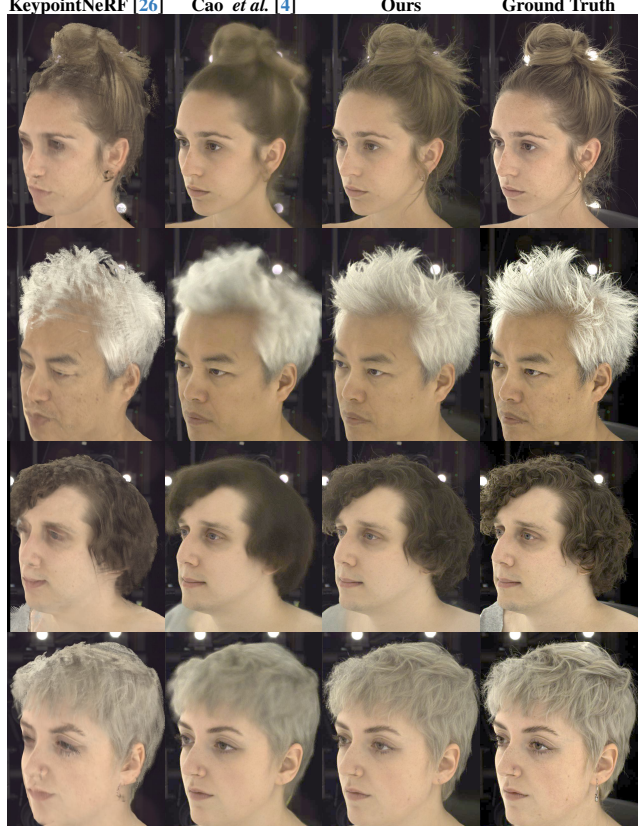


**Figure 2. Novel View Synthesis.** Rendering results on the holdout views of the training identities. We compare our method with KeypointNeRF [26] and Cao *et al.* [4]. Our method is compatible with different hair geometries and captures the detailed volumetric texture of varied hairstyles. Please refer to the supplemental materials for more rendering results and comparisons.

TRAIN	MSE( $\downarrow$ )	PSNR( $\uparrow$ )	SSIM( $\uparrow$ )	LPIPS( $\downarrow$ )
KeypointNeRF [26]	257.42	24.57	0.86	0.3140
Cao <i>et al.</i> [4]	159.37	27.12	0.7961	0.3117
Ours	<b>130.07</b>	<b>27.73</b>	<b>0.8922</b>	<b>0.1993</b>
TEST	MSE( $\downarrow$ )	PSNR( $\uparrow$ )	SSIM( $\uparrow$ )	LPIPS( $\downarrow$ )
KeypointNeRF [26]	303.60	23.77	0.8596	0.3389
Cao <i>et al.</i> [4]	334.68	23.89	0.7883	0.3511
Ours	<b>236.46</b>	<b>25.08</b>	<b>0.8741</b>	<b>0.2610</b>

**Table 1. Novel View Synthesis.** We show qualitative results on novel view synthesis. The upper part and lower part of the table report the MSE, PSNR, SSIM and LPIPS computed on the holdout views of training identities and the test identities respectively. Our method achieves a better result on MSE, PSNR and SSIM compared to previous methods [4, 26]. Our method is capable of generating sharp appearance on detailed geometries which leads to improvement on LPIPS by a large margin.

each model reconstructs the appearance and shape of the head and hair from those training identities. Compared to

KeypointNeRF [26], we achieve a lower distortion in terms of reconstructing different hairstyles. When compared with the UPM model [4], we find that our model enjoys a much larger improvement on LPIPS compared to the other reconstruction metrics like MSE, PSNR and SSIM. One of the reasons behind this result is that the perceptual metric is more sensitive to high-frequency information as well as the fine-level details in one’s appearance. The UPM model is capable of reconstructing a coarse-level geometry and appearance but fails to capture the fine-level details which our model does a better job on. Furthermore, the UPM model is inherently limited by its use of a mesh to represent complex hair topology, even at a coarse level. In Fig. 2, the improvements of our methods can be better justified visually, where we show the rendering results of each method on the holdout views of several training identities. On the lower part of Tab. 1, we report the metrics computed on the same set of holdout views but of test identities. Fig. 3 shows the rendering results of some of those views. We can see that the UPM model [4] and ours both achieve better generalization on the face than KeypointNeRF [26] as a result of having awareness of face geometry. While pixel-aligned information from multi-view images is used as input for KeypointNeRF, learning a generalizable network to triangulate these 2D observations can be challenging, particularly for diverse geometries. Our method can achieve a more detailed hair appearance given sparse inputs like point clouds on never-seen-before identities.

**Ablation on input features  $\Omega^{\rho_i}$ ,  $\Gamma^{\rho_i}$  and  $\Lambda^{\rho_i}$ .** We ablate on the usage of different input features to the local appearance networks  $\Psi_\alpha(\cdot)$  and  $\Psi_{rgb}(\cdot)$ . Tab. 2 shows the performance of our model under different input configurations. The base model is  $\Psi_\alpha(\Omega^{\rho_i}) + \Psi_{rgb}(\Omega^{\rho_i}, \hat{c})$ , which only takes  $\Omega^{\rho_i}$  and  $\hat{c}$  as input and do not have untied bias for each layer.  $+\Gamma^\rho$  represents the model that use  $\Gamma^\rho$  as additional input to both  $\Psi_\alpha(\cdot)$  and  $\Psi_{rgb}(\cdot)$ .  $+ub$  stands for adding untied bias to each learnable layer in  $\Psi_\alpha(\cdot)$  and  $\Psi_{rgb}(\cdot)$ .

According to Tab. 2, the inclusion of  $\Gamma^\rho$  helps the base model to converge better with improved image reconstruction and perceptual metrics on both training and testing sets. However, adding untied bias solely gives worse results on both data splits. We argue that using  $\Omega^\rho$  as the only input makes the network to be aware of only local region and to be agnostic of positional information, which further exposes the network to the noise in  $\Omega^\rho$ . Including additional network parameters like the untied bias in such a setting will make the network even harder to learn. If we combine both  $\Gamma^\rho$  and the untied bias, we get much better performance on the training set. This improvement suggests that using  $\Gamma^\rho$  is more effective than just adding more network parameters, which helps the network to capture the underlying correlation between human hair’s appearance and spatial position. Finally, we find that having per-vertex view conditioning  $\Lambda^\rho$



**Figure 3. Novel View Synthesis.** Rendering results on the test identities. We compare our method with KeypointNeRF [26] and Cao *et al.* [4]. Our method generalizes reasonably to new identities and is capable of generating a photorealistic appearance without any finetuning. Please refer to the supplemental materials for more rendering results and comparisons.

as additional input help the model to achieve the best performance on both the training and testing set. As different hair geometry leads to different shadow and reflectance patterns, the per-vertex viewing condition  $\Lambda^\rho$  serves as a more informative term than the viewing direction  $\hat{c}$  to infer the view-conditioned appearance.

**Ablation on finetuning efficiency.** Even though our model generalizes reasonably to unseen identities and creates photorealistic avatars for them, finetuning or online optimization is still needed for getting metrically correct personalized avatars. Thus, we evaluate our model in terms of how well it can help get personalized avatars for novel identities efficiently. Given RGB-D scans of new subjects with novel hairstyles, we finetune our model based on them to capture the personalized 3D avatar. We ablate on both the number of views needed to do finetuning as well as the number of iterations we update our model.

In Fig 5, we show how MSE, PSNR, SSIM and LPIPS on test views change across optimization steps. Each curve in

	TRAIN				TEST			
	MSE( $\downarrow$ )	PSNR( $\uparrow$ )	SSIM( $\uparrow$ )	LPIPS( $\downarrow$ )	MSE( $\downarrow$ )	PSNR( $\uparrow$ )	SSIM( $\uparrow$ )	LPIPS( $\downarrow$ )
base	150.69	27.11	0.8090	0.2039	242.56	25.01	0.8023	0.2556
base+ $\Gamma^{\rho}$	140.38	27.42	0.8123	0.1973	228.41	25.19	0.8059	0.2479
base+ub	164.04	26.70	0.8022	0.2234	253.61	24.69	0.7969	0.2705
base+ $\Gamma^{\rho}$ +ub	134.60	27.54	0.8108	0.2042	236.46	25.08	0.8081	0.2610
base+ $\Gamma^{\rho}$ +ub+ $\Lambda^{\rho}$	130.07	27.73	0.8922	0.1993	220.00	25.45	0.8741	0.2472

Table 2. **Ablation on different inputs**  $\Omega^{\rho_i}$ ,  $\Gamma^{\rho_i}$  and  $\Lambda^{\rho_i}$ . We evaluate models with different input configurations and report their MSE, PSNR, SSIM and LPIPS on the holdout views of both training and testing data. As we can see, both  $\Gamma^{\rho_i}$  and  $\Lambda^{\rho_i}$  serve as a more effective way to improve the model performance compared to just increasing the model’s capacity like with untied bias  $ub$ . We also find that the inclusion of per-vertex viewing direction  $\Lambda^{\rho_i}$  improves the model’s performance on novel view synthesis by a large margin. We use **gold**, **silver** and **bronze** to indicate first, second and third places.

Fig 5 represents a model with a different finetuning configuration.  $ft$  stands for finetuning a pre-trained model on the new identity while  $noft$  stands for training the same model on the new identity from scratch.  $xvs$  indicates that we use a total number of  $x$  views to perform the finetuning. For example, 10vs means that we use 10 views for finetuning. To make sure that the finetuning views are not biased to certain viewpoints, we sample the finetuning views from all training views using the furthest point sampling. As we can see, the pre-trained model could give the finetuning a warm start and leads to better convergence under a short amount of training time, which is also robust to the density of finetuning views.

In Fig 4, we show the rendering results of a test view under different finetuning/training configurations as in Fig. 5. As we can see, at iteration 0, our model can already reconstruct most details about the new hairstyle and after 100 iterations models trained with different numbers of views gets sharp results, while models trained from scratch have not yet converged.

## 4.2. Personalized Avatar from an iPhone Scan

We demonstrate an application enabled by our method, which is the efficient generation of personalized avatars with an iPhone scan. We used a multi-view camera system to collect the training and validation data for learning the local appearance prior model  $\Psi_{\alpha}$  and  $\Psi_{rgb}$ . However, a multi-view capture system is expensive to set up and not readily available to create personalized avatars for individuals. To accommodate the need for simplicity and scalability, we seek to use a single RGB-D camera (like an iPhone) to substitute for the multi-view capture system. We demonstrate that our learned model  $\Psi_{\alpha}$  and  $\Psi_{rgb}$  can infill the gaps between in-the-wild capture and a lab-level capture accommodate a sparse view and noisy camera tracking setup.

**Reconstructing from iPhone Scan.** We perform further

experiments on reconstructing a personalized avatar from an iPhone scan in sparse views. The data we used is RGB-D data from the iPhone scan. We asked the participant to sit still and start our iPhone scan by facing the iPhone towards the participant at a distance of 30-50cm and capturing different perspectives of the participant’s face, which results in the participant occupying 70 – 80% of the whole image. The resolution of the captured image is  $1024 \times 667$  and the resolution of the captured depth image is  $640 \times 480$ . To get the iPhone tracking information, we perform ICP tracking using the per-frame depth as well as color information from the RGB-D scan under different perspectives. Given the nature of the in-the-wild capture setup, there will be noise in both the depth scan as well as the camera tracking. We demonstrate that our method is not severely affected by those sources of noise.

We compare our method with instant-npg [28] based on the implementation [42] and perform personalized avatar acquisition from the RGB-D scan. We optimize both instant-npg and our method using five views with training objectives described in Sec 3.2. To prepare the input to our method, we fuse the RGB-D scans into a point cloud given the ICP tracking results. We generate the foreground mask using RVM [19] and masked the background in the iPhone captures to be black with the mask. Both models are optimized for 5min and converge. As shown in Fig. 6, our method and instant-npg create good-quality rendering on the training views. However, we also find that instant-npg yields floating artifacts under the sparse view training setting. When we render from a camera view not in the training set, the quality of instant-npg decays dramatically. This result suggests that our method is more robust to sparse views training and camera tracking noise with fewer floating artifacts and suffers from less overfitting on training views.



**Figure 4. Rendering results under different finetuning steps and views.** We show finetuned results under iteration 0 and 100 on the first and third columns respectively and train from scratch results on the second and fourth. From left to right, the results are from models trained using 10, 20, 40 and 80 views. In the lower right corner, we show the ground truth image under the rendering view for reference.

## 5. Conclusion

In this paper, we develop a method based on compositional volumetric representation for efficient and accurate capturing of human avatars with diverse hairstyles. Towards that goal, we build a universal hair appearance prior model for modeling the appearance of diverse hairstyles. To accommodate the large intra-class variance in hair appearance, we split hairstyles into small volumetric primitives and learn a local appearance model that captures the universal appearance prior at that scale. We empirically show that our model is capable of generating a dense radiance field for a large spectrum of hairstyles with photorealistic appearance and outperforms previous state-of-the-art approaches on both capturing fidelity and generalization. As a result,

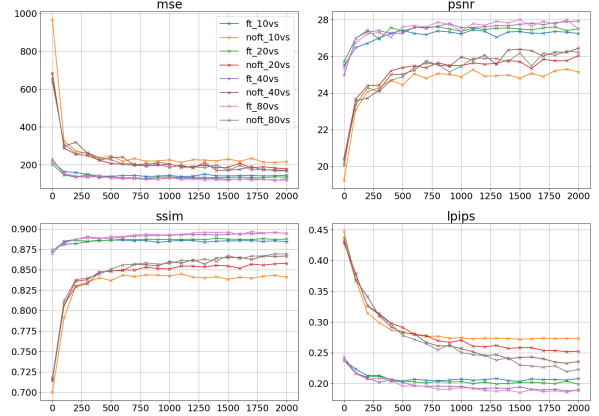


**Figure 5. Ablation on different finetuning configurations.** We show the learning curve of models under different finetuning configurations. We finetune(ft) our model as well as train from scratch(noft) with a varied number of training views in  $\{10, 20, 40, 80\}$  that are approximately uniformly sampled from all training views. Our pre-trained model creates a warm start for avatar personalization and is also robust to the number of views used for finetuning.

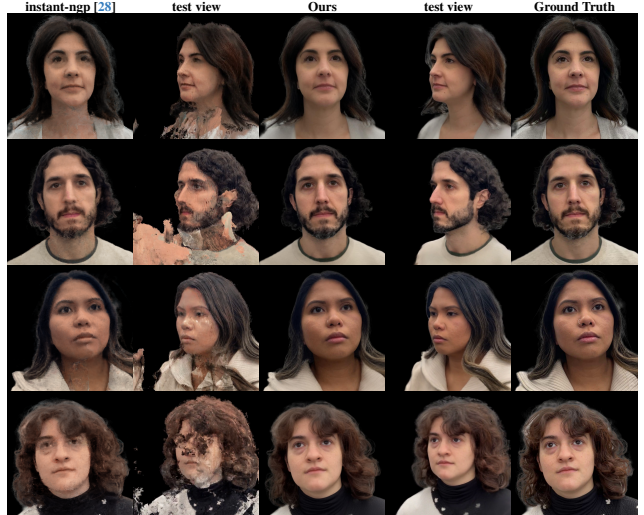


**Figure 6. Rendering results on iPhone captured data.** We show the results of our method and instant-npg on the iPhone-captured data. Both our method and instant-npg work well on the training views while our method works better on testing views

our method supports applications like generating personalized avatars from in-the-wild scans using sparse views. However, our model is limited to static hair and does not support relighting. How to extend the current model for those purposes are interesting future problems.

## References

- [1] Jonathan T Barron, Ben Mildenhall, Matthew Tancik, Peter Hedman, Ricardo Martin-Brualla, and Pratul P Srinivasan. Mip-nerf: A multiscale representation for anti-aliasing neural radiance fields. In *Proceedings of the IEEE/CVF International Conference on Computer Vision*, pages 5855–5864, 2021. [2](#)
- [2] Jonathan T Barron, Ben Mildenhall, Dor Verbin, Pratul P Srinivasan, and Peter Hedman. Mip-nerf 360: Unbounded anti-aliased neural radiance fields. In *Proceedings of the IEEE/CVF Conference on Computer Vision and Pattern Recognition*, pages 5470–5479, 2022.
- [3] Jonathan T Barron, Ben Mildenhall, Dor Verbin, Pratul P Srinivasan, and Peter Hedman. Zip-nerf: Anti-aliased grid-based neural radiance fields. *arXiv preprint arXiv:2304.06706*, 2023. [2](#)
- [4] Chen Cao, Tomas Simon, Jin Kyu Kim, Gabe Schwartz, Michael Zollhoefer, Shun-Suke Saito, Stephen Lombardi, Shih-En Wei, Danielle Belko, Shouo-I Yu, Yaser Sheikh, and Jason Saragih. Authentic volumetric avatars from a phone scan. *ACM Transactions on Graphics*, 41(4), 2022. [2, 3, 5, 6](#)
- [5] Menglei Chai, Lvdi Wang, Yanlin Weng, Yizhou Yu, Baining Guo, and Kun Zhou. Single-view hair modeling for portrait manipulation. *ACM Transactions on Graphics (TOG)*, 31(4):1–8, 2012. [2](#)
- [6] Menglei Chai, Tianjia Shao, Hongzhi Wu, Yanlin Weng, and Kun Zhou. Autohair: Fully automatic hair modeling from a single image. *ACM Transactions on Graphics*, 35(4), 2016. [2](#)
- [7] Anpei Chen, Zexiang Xu, Fuqiang Zhao, Xiaoshuai Zhang, Fanbo Xiang, Jingyi Yu, and Hao Su. Mvsnerf: Fast generalizable radiance field reconstruction from multi-view stereo. In *Proceedings of the IEEE/CVF International Conference on Computer Vision*, pages 14124–14133, 2021. [3](#)
- [8] Anpei Chen, Zexiang Xu, Andreas Geiger, Jingyi Yu, and Hao Su. Tensorf: Tensorial radiance fields. In *European Conference on Computer Vision*, pages 333–350. Springer, 2022. [2](#)
- [9] Guy Gafni, Justus Thies, Michael Zollhöfer, and Matthias Nießner. Dynamic neural radiance fields for monocular 4d facial avatar reconstruction. In *Proceedings of the IEEE/CVF Conference on Computer Vision and Pattern Recognition*, pages 8649–8658, 2021. [1, 3](#)
- [10] Philip-William Grassal, Malte Prinzler, Titus Leistner, Carsten Rother, Matthias Nießner, and Justus Thies. Neural head avatars from monocular rgb videos. In *Proceedings of the IEEE/CVF Conference on Computer Vision and Pattern Recognition*, pages 18653–18664, 2022.
- [11] Yang Hong, Bo Peng, Haiyao Xiao, Ligang Liu, and Juyong Zhang. Headnerf: A real-time nerf-based parametric head model. In *Proceedings of the IEEE/CVF Conference on Computer Vision and Pattern Recognition*, pages 20374–20384, 2022. [1, 3](#)
- [12] Liwen Hu, Chongyang Ma, Linjie Luo, and Hao Li. Robust hair capture using simulated examples. *ACM Transactions on Graphics*, 33(4):1–10, 2014. [2](#)
- [13] Liwen Hu, Chongyang Ma, Linjie Luo, and Hao Li. Single-view hair modeling using a hairstyle database. *ACM Transactions on Graphics (ToG)*, 34(4):1–9, 2015. [2](#)
- [14] Kacper Kania, Kwang Moo Yi, Marek Kowalski, Tomasz Trzcinski, and Andrea Tagliasacchi. CoNeRF: Controllable Neural Radiance Fields. In *Proceedings of the IEEE Conference on Computer Vision and Pattern Recognition*, 2022. [1, 3](#)
- [15] Anastasiia Kornilova, Marsel Faizullin, Konstantin Pakulev, Andrey Sadkov, Denis Kukushkin, Azat Akhmetyanov, Timur Akhtyamov, Hekmat Tahernejad, and Gonzalo Ferrer. Smartportraits: Depth powered handheld smartphone dataset of human portraits for state estimation, reconstruction and synthesis. In *Proceedings of the IEEE/CVF Conference on Computer Vision and Pattern Recognition*, pages 21318–21329, 2022. [1, 3](#)
- [16] Zhiyi Kuang, Yiyang Chen, Hongbo Fu, Kun Zhou, and Youyi Zheng. Deepmvhair: Deep hair modeling from sparse views. In *SIGGRAPH Asia 2022 Conference Papers*, pages 1–8, 2022. [2](#)
- [17] Tianye Li, Timo Bolkart, Michael J Black, Hao Li, and Javier Romero. Learning a model of facial shape and expression from 4d scans. *ACM Transactions on Graphics*, 36(6):194–1, 2017. [3](#)
- [18] Shu Liang, Xiufeng Huang, Xianyu Meng, Kunyao Chen, Linda G Shapiro, and Ira Kemelmacher-Shlizerman. Video to fully automatic 3d hair model. *ACM Transactions on Graphics (TOG)*, 37(6):1–14, 2018. [2](#)
- [19] Shanchuan Lin, Linjie Yang, Imran Saleemi, and Soumyadip Sengupta. Robust high-resolution video matting with temporal guidance. In *Proceedings of the IEEE/CVF Winter Conference on Applications of Computer Vision*, pages 238–247, 2022. [7](#)
- [20] David B Lindell, Julien NP Martel, and Gordon Wetzstein. Autoint: Automatic integration for fast neural volume rendering. In *Proceedings of the IEEE/CVF Conference on Computer Vision and Pattern Recognition*, pages 14556–14565, 2021. [2](#)
- [21] Lingjie Liu, Jitao Gu, Kyaw Zaw Lin, Tat-Seng Chua, and Christian Theobalt. Neural sparse voxel fields. In *Advances in Neural Information Processing Systems*. Curran Associates, Inc., 2020. [2](#)
- [22] Stephen Lombardi, Tomas Simon, Jason Saragih, Gabriel Schwartz, Andreas Lehrmann, and Yaser Sheikh. Neural volumes: Learning dynamic renderable volumes from images. *ACM Transactions on Graphics*, 38(4), 2019. [2](#)
- [23] Stephen Lombardi, Tomas Simon, Gabriel Schwartz, Michael Zollhoefer, Yaser Sheikh, and Jason Saragih. Mixture of volumetric primitives for efficient neural rendering. *ACM Transactions on Graphics*, 40(4), 2021. [3, 4, 1](#)
- [24] Linjie Luo, Hao Li, Sylvain Paris, Thibaut Weise, Mark Pauly, and Szymon Rusinkiewicz. Multi-view hair capture using orientation fields. In *Proceedings of the IEEE/CVF Conference on Computer Vision and Pattern Recognition*, pages 1490–1497. IEEE, 2012. [2](#)
- [25] Linjie Luo, Cha Zhang, Zhengyou Zhang, and Szymon Rusinkiewicz. Wide-baseline hair capture using strand-based

refinement. In *Proceedings of the IEEE/CVF Conference on Computer Vision and Pattern Recognition*, pages 265–272, 2013. 2

[26] Marko Mihajlovic, Aayush Bansal, Michael Zollhoefer, Siyu Tang, and Shunsuke Saito. KeypointNeRF: Generalizing image-based volumetric avatars using relative spatial encoding of keypoints. In *European conference on computer vision*, 2022. 2, 3, 5, 6

[27] Ben Mildenhall, Pratul P Srinivasan, Matthew Tancik, Jonathan T Barron, Ravi Ramamoorthi, and Ren Ng. Nerf: Representing scenes as neural radiance fields for view synthesis. In *European Conference on Computer Vision*. Springer, 2020. 2

[28] Thomas Müller, Alex Evans, Christoph Schied, and Alexander Keller. Instant neural graphics primitives with a multiresolution hash encoding. *ACM Trans. Graph.*, 41(4):102:1–102:15, 2022. 2, 3, 7, 8

[29] Giljoo Nam, Chenglei Wu, Min H Kim, and Yaser Sheikh. Strand-accurate multi-view hair capture. In *Proceedings of the IEEE/CVF Conference on Computer Vision and Pattern Recognition*, pages 155–164, 2019. 2

[30] Michael Oechsle, Songyou Peng, and Andreas Geiger. Unisurf: Unifying neural implicit surfaces and radiance fields for multi-view reconstruction. In *Proceedings of the IEEE/CVF International Conference on Computer Vision*, pages 5589–5599, 2021. 2

[31] Sylvain Paris, Hector M Briceno, and François X Sillion. Capture of hair geometry from multiple images. *ACM Transactions on Graphics*, 23(3):712–719, 2004. 2

[32] Sylvain Paris, Will Chang, Oleg I Kozhushnyan, Wojciech Jarosz, Wojciech Matusik, Matthias Zwicker, and Frédo Durand. Hair photobooth: geometric and photometric acquisition of real hairstyles. *ACM Transactions on Graphics*, 27(3):30, 2008. 2

[33] Keunhong Park, Utkarsh Sinha, Jonathan T Barron, Sofien Bouaziz, Dan B Goldman, Steven M Seitz, and Ricardo Martin-Brualla. Nerfies: Deformable neural radiance fields. In *Proceedings of the IEEE/CVF International Conference on Computer Vision*, pages 5865–5874, 2021. 1, 3

[34] Keunhong Park, Utkarsh Sinha, Peter Hedman, Jonathan T. Barron, Sofien Bouaziz, Dan B Goldman, Ricardo Martin-Brualla, and Steven M. Seitz. Hypernerf: A higher-dimensional representation for topologically varying neural radiance fields. *arXiv preprint arXiv:2106.13228*, 2021. 1, 3

[35] Charles R Qi, Hao Su, Kaichun Mo, and Leonidas J Guibas. Pointnet: Deep learning on point sets for 3d classification and segmentation. In *Proceedings of the IEEE/CVF Conference on Computer Vision and Pattern Recognition*, 2017. 4

[36] Amit Raj, Michael Zollhoefer, Tomas Simon, Jason Saragih, Shunsuke Saito, James Hays, and Stephen Lombardi. Pixel-aligned volumetric avatars. In *Proceedings of the IEEE/CVF Conference on Computer Vision and Pattern Recognition*, pages 11733–11742, 2021. 3

[37] Christian Reiser, Songyou Peng, Yiyi Liao, and Andreas Geiger. Kilonerf: Speeding up neural radiance fields with thousands of tiny mlps. In *Proceedings of the IEEE/CVF International Conference on Computer Vision*, pages 14335–14345, 2021. 2

[38] Olaf Ronneberger, Philipp Fischer, and Thomas Brox. U-net: Convolutional networks for biomedical image segmentation. In *International Conference on Medical image computing and computer-assisted intervention*, pages 234–241. Springer, 2015. 4

[39] Radu Alexandru Rosu, Shunsuke Saito, Ziyan Wang, Chenglei Wu, Sven Behnke, and Giljoo Nam. Neural strands: Learning hair geometry and appearance from multi-view images. In *European Conference on Computer Vision*, pages 73–89. Springer, 2022. 2

[40] Shunsuke Saito, Liwen Hu, Chongyang Ma, Hikaru Ibayashi, Linjie Luo, and Hao Li. 3d hair synthesis using volumetric variational autoencoders. *ACM Transactions on Graphics (TOG)*, 37(6):1–12, 2018. 2

[41] Tiancheng Sun, Giljoo Nam, Carlos Aliaga, Christophe Hery, and Ravi Ramamoorthi. Human Hair Inverse Rendering using Multi-View Photometric data. In *Eurographics Symposium on Rendering - DL-only Track*. The Eurographics Association, 2021. 2

[42] Jiaxiang Tang. Torch-npg: a pytorch implementation of instant-npg, 2022. <https://github.com/ashawkey/torch-npg>. 7

[43] Peng Wang, Lingjie Liu, Yuan Liu, Christian Theobalt, Taku Komura, and Wenping Wang. Neus: Learning neural implicit surfaces by volume rendering for multi-view reconstruction. *NeurIPS*, 2021. 2

[44] Ziyang Wang, Timur Bagautdinov, Stephen Lombardi, Tomas Simon, Jason Saragih, Jessica Hodgins, and Michael Zollhoefer. Learning compositional radiance fields of dynamic human heads. In *Proceedings of the IEEE/CVF Conference on Computer Vision and Pattern Recognition*, pages 5704–5713, 2021. 2

[45] Ziyan Wang, Giljoo Nam, Tuur Stuyck, Stephen Lombardi, Michael Zollhoefer, Jessica Hodgins, and Christoph Lassner. Hvh: Learning a hybrid neural volumetric representation for dynamic hair performance capture, 2021. 1, 3

[46] Ziyang Wang, Giljoo Nam, Tuur Stuyck, Stephen Lombardi, Chen Cao, Jason Saragih, Michael Zollhöfer, Jessica Hodgins, and Christoph Lassner. Neuwig: A neural dynamic model for volumetric hair capture and animation. In *Proceedings of the IEEE/CVF Conference on Computer Vision and Pattern Recognition*, pages 8641–8651, 2023. 3, 4, 1

[47] Yichen Wei, Eyal Ofek, Long Quan, and Heung-Yeung Shum. Modeling hair from multiple views. In *ACM SIGGRAPH 2005 Papers*, pages 816–820. 2005. 2

[48] Keyu Wu, Yifan Ye, Lingchen Yang, Hongbo Fu, Kun Zhou, and Youyi Zheng. Neuralhdhair: Automatic high-fidelity hair modeling from a single image using implicit neural representations. In *Proceedings of the IEEE/CVF Conference on Computer Vision and Pattern Recognition*, pages 1526–1535, 2022. 2

[49] Lingchen Yang, Zefeng Shi, Youyi Zheng, and Kun Zhou. Dynamic hair modeling from monocular videos using deep neural networks. *ACM Transactions on Graphics*, 38(6):1–12, 2019. 2

[50] Lior Yariv, Jiatao Gu, Yoni Kasten, and Yaron Lipman. Volume rendering of neural implicit surfaces. In *Thirty-Fifth Conference on Neural Information Processing Systems*, 2021. 2

[51] Alex Yu, Ruilong Li, Matthew Tancik, Hao Li, Ren Ng, and Angjoo Kanazawa. Plenoctrees for real-time rendering of neural radiance fields. In *Proceedings of the IEEE/CVF International Conference on Computer Vision*, pages 5752–5761, 2021. 2

[52] Alex Yu, Vickie Ye, Matthew Tancik, and Angjoo Kanazawa. pixelnerf: Neural radiance fields from one or few images. In *Proceedings of the IEEE/CVF Conference on Computer Vision and Pattern Recognition*, pages 4578–4587, 2021. 3

[53] Meng Zhang and Youyi Zheng. Hair-gans: Recovering 3d hair structure from a single image. *arXiv preprint arXiv:1811.06229*, 2018. 2

[54] Yufeng Zheng, Victoria Fernández Abrevaya, Marcel C. Bühlert, Xu Chen, Michael J. Black, and Otmar Hilliges. I m avatar: Implicit morphable head avatars from videos. In *Proceedings of the IEEE/CVF Conference on Computer Vision and Pattern Recognition*, pages 13545–13555, 2022. 1, 3

[55] Yujian Zheng, Zirong Jin, Moran Li, Haibin Huang, Chongyang Ma, Shuguang Cui, and Xiaoguang Han. Hairstep: Transfer synthetic to real using strand and depth maps for single-view 3d hair modeling. In *Proceedings of the IEEE/CVF Conference on Computer Vision and Pattern Recognition*, pages 12726–12735, 2023. 2

[56] Yufeng Zheng, Wang Yifan, Gordon Wetzstein, Michael J Black, and Otmar Hilliges. Pointavatar: Deformable point-based head avatars from videos. In *Proceedings of the IEEE/CVF Conference on Computer Vision and Pattern Recognition*, pages 21057–21067, 2023. 1, 3

[57] Yi Zhou, Liwen Hu, Jun Xing, Weikai Chen, Han-Wei Kung, Xin Tong, and Hao Li. Hairnet: Single-view hair reconstruction using convolutional neural networks. In *Proceedings of the European Conference on Computer Vision (ECCV)*, pages 235–251, 2018. 2

[58] Wojciech Zienonka, Timo Bolkart, and Justus Thies. Instant volumetric head avatars. In *Proceedings of the IEEE/CVF Conference on Computer Vision and Pattern Recognition*, pages 4574–4584, 2023. 3

# A Local Appearance Model for Volumetric Capture of Diverse Hairstyles

## Supplementary Material

### 6. Implementation Details on Volumetric Renndering

**Differentiable Volumetric Raymarching.** Following the formulation in Sec 3.1, we first explain the implementation details regarding how we aggregate the spatial radiance functions  $\mathbf{V}_{rgb}$ ,  $\mathbf{V}_\alpha$  and  $\mathbf{V}_{label}$  into the renderings as  $\mathcal{I}_p$ ,  $\mathcal{M}_p$  and  $T(l)$ . We use Riemann sum to approximate the integral in Sec 3.1. For simplicity, we use a toy example shown in Figure 7 for easier illustration. We denote the

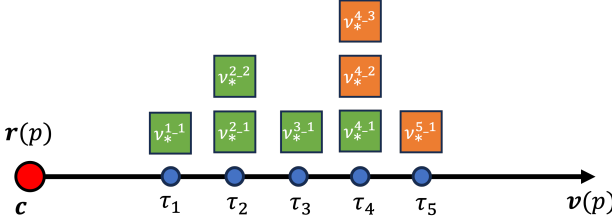


Figure 7. Raymarching example.

red dot  $c$  as the camera center and the arrow  $v(p)$  as the raymarching direction of pixel  $p$ . We march the ray with uniform step size which results in sample points (blue dots) along the ray with depth  $\tau_i$ . And we denote the volumetric primitives that intersect with those sample points as  $\nu_*^j$  where  $*$  can be  $\alpha$ ,  $rgb$  or  $label$  and  $j$  is the index of the corresponding volumetric primitive. The green ones are the primitives for the non-hair region and the orange ones are the primitives for the hair region. We use the term  $\nu_*^j(\tau_i)$  as the value we sampled from  $\nu_*^j$  at point  $\tau_i$ . To get  $\nu_*^j(\tau_i)$ , we use trilinear interpolation between the nearest grid points of  $\tau_i$  in  $\nu_*^j$ . As in MVP, the aggregated  $\alpha$  value up to  $\tau_i$  along the ray is computed as below

$$T(\tau_i) = \min(1, \sum_{j=1}^i \sum_{k \in j_k} \nu_\alpha^{j,k}),$$

where  $j_k$  is the set for all the indices of the intersected primitives at  $\tau_j$ . Supposing that all the  $\alpha$  values adds up to a value greater than 1 at  $\nu_\alpha^{4,1}$ , we will have

$$\begin{aligned} T(\tau_1) &= \nu_\alpha^{1,1} \\ T(\tau_2) &= T(\tau_1) + \nu_\alpha^{2,1} + \nu_\alpha^{2,2} \\ T(\tau_3) &= T(\tau_2) + \nu_\alpha^{3,1} \\ T(\tau_4) &= 1 \\ T(\tau_5) &= 1, \end{aligned}$$

where  $T(\tau_4)$  and  $T(\tau_5)$  will be constant. Thus, we will have the aggregated  $rgb$  and  $label$  values in MVP [23] as

$$\begin{aligned} \mathcal{I}_p^{non-soft} &= \nu_\alpha^{1,1} \nu_{rgb}^{1,1} + \nu_\alpha^{2,1} \nu_{rgb}^{2,1} + \nu_\alpha^{2,2} \nu_{rgb}^{2,2} \\ &\quad + \nu_\alpha^{3,1} \nu_{rgb}^{3,1} + (1 - T(\tau_3)) \nu_{rgb}^{4,1} \\ \mathcal{M}_p^{non-soft} &= 0, \end{aligned}$$

where the above equation will yield 0 gradient with respect to  $\nu_*^{4,2}$ ,  $\nu_*^{4,3}$  and  $\nu_*^{5,1}$ . As in NeuWigs [46], the aggregated label value will be zero in this case as  $T(\cdot)$  already saturates at  $\nu_\alpha^{4,1}$  and will not keep aggregating values from  $\nu_*^{4,2}$  and  $\nu_*^{4,3}$  even though they are at the same point. This early termination of raymarching is guided by the stochasticity in primitive sorting and is especially problematic if pixel  $p$  is on the hair region. In this case, the label loss will not back-propagate any useful gradients to update  $\nu_\alpha^i$  to the correct value. To fix that problem, we make the saturation point to be better aware of the other intersecting boxes with a new soft blending formulation. Instead of taking the RGB and label value of the very first box  $\tau_4$  intersects, we compute the RGB and label at that point as

$$\begin{aligned} \mathcal{I}_p^{soft} &= \nu_\alpha^{1,1} \nu_{rgb}^{1,1} + \nu_\alpha^{2,1} \nu_{rgb}^{2,1} \\ &\quad + \nu_\alpha^{2,2} \nu_{rgb}^{2,2} + \nu_\alpha^{3,1} \nu_{rgb}^{3,1} \\ &\quad + (1 - T(\tau_3)) \frac{\sum_{i=1}^3 \nu_\alpha^{4,i} \nu_{rgb}^{4,i}}{\sum_{i=1}^3 \nu_\alpha^{4,i}} \\ \mathcal{M}_p^{soft} &= (1 - T(\tau_3)) \frac{\sum_{i=2}^3 \nu_\alpha^{4,i}}{\sum_{i=1}^3 \nu_\alpha^{4,i}}. \end{aligned}$$

With a soft blending reformulation, the rendering terms  $\mathcal{I}_p^{soft}$  and  $\mathcal{M}_p^{soft}$  are both aware of all the primitives intersected at the saturation point and the rendering formulation is no longer affected by the stochasticity in the primitive sorting at the same point. The new formulation with soft blending is more robust to different initialization on the poses of hair and non-hair primitives. Specifically, we write

the gradients of each  $\nu_*^{4-1}$  below,

$$\begin{aligned} \frac{\partial \mathcal{I}_p^{non-soft}}{\partial \nu_\alpha^{4-1}} &= 0 \\ \frac{\partial \mathcal{I}_p^{non-soft}}{\partial \nu_{rgb}^{4-1}} &= 1 - T(\tau_3) \\ \frac{\partial \mathcal{M}_p^{non-soft}}{\partial \nu_\alpha^{4-1}} &= 0 \\ \frac{\partial \mathcal{I}_p^{soft}}{\partial \nu_\alpha^{4-1}} &= (1 - T(\tau_3)) \frac{\sum_{i=2}^3 (\nu_{rgb}^{4-i} - \nu_{rgb}^{4-1}) \nu_\alpha^{4-i}}{(\sum_{i=1}^3 \nu_\alpha^{4-i})^2} \\ \frac{\partial \mathcal{I}_p^{soft}}{\partial \nu_{rgb}^{4-1}} &= (1 - T(\tau_3)) \frac{\nu_\alpha^{4-1}}{\sum_{i=1}^3 \nu_\alpha^{4-i}} \\ \frac{\partial \mathcal{M}_p^{soft}}{\partial \nu_\alpha^{4-1}} &= -(1 - T(\tau_3)) \frac{1}{(\sum_{i=1}^3 \nu_\alpha^{4-i})^2}, \end{aligned}$$

where you can see the soft blending version has a more meaningful gradient where  $\frac{\partial \mathcal{I}_p^{soft}}{\partial \nu_\alpha^{4-1}}$  and  $\frac{\partial \mathcal{M}_p^{soft}}{\partial \nu_\alpha^{4-1}}$  are not zero but are jointly determined by all primitives at  $\tau_4$ . Given the symmetry between  $\nu_*^{4-i}$ , the gradients of  $\nu_*^{4-2}$  and  $\nu_*^{4-3}$  are the same to  $\nu_*^{4-1}$  except that

$$\frac{\partial \mathcal{M}_p^{soft}}{\partial \nu_\alpha^{4-2}} = (1 - T(\tau_3)) \frac{\nu_\alpha^{4-1}}{(\sum_{i=1}^3 \nu_\alpha^{4-i})^2}.$$

Given the gradients  $\frac{\partial \mathcal{M}_p^{soft}}{\partial \nu_\alpha^{4-i}}$ , we will find that the primitives with a zero label will be updated inverse proportional to how  $\mathcal{M}_p^{soft}$  changes while primitives with a non-zero label will change proportionally with respect to  $\mathcal{M}_p^{soft}$ .

## 7. Training details

We formulate the training objective  $\mathcal{L}$  as below:

$$\mathcal{L} = \mathcal{L}_1 + \lambda_{VGG} \mathcal{L}_{VGG} + \lambda_{seg} \mathcal{L}_{seg},$$

where  $\lambda_{VGG}$  and  $\lambda_{seg}$  are positive values for rebalancing each term in the training objectives. The first term  $\mathcal{L}_1$  measures the difference between the rendered image  $\tilde{\mathcal{I}}$  and the ground truth image  $I_{gt}$ :

$$\mathcal{L}_1 = \|\tilde{\mathcal{I}} - I_{gt}\|_1.$$

To enhance the rendering fidelity and achieve better convergence on  $\mathcal{L}_1$ , we add a second term of perceptual loss as

$$\mathcal{L}_{VGG} = \sum_i \|VGG_i(\tilde{\mathcal{I}}) - VGG_i(I_{gt})\|_1,$$

where  $VGG_i(\cdot)$  indicates extracting the intermediate feature from the  $i$ th layer of a pretrained VGG network. The last term  $\mathcal{L}_{seg}$  is segmentation loss,

$$\mathcal{L}_{seg} = \|\mathcal{M} - M_{gt}\|_1,$$

which is the  $L_1$  distance between the rendered mask  $\mathcal{M}$  and the ground truth segmentation mask  $M_{gt}$ .

To mitigate overfitting, we perform data augmentation while training. In order to mimic the noise pattern in the input point cloud, we randomly jitter each point in the point cloud  $q$  with Gaussian noise. We find that data augmentation helps stabilize the training.

## 8. More Rendering Results

We show the rendering results in Fig. 8 and Fig. 9 and visualize the input sparse point cloud of more hairstyles in Fig. 10 and Fig. 11. As we can see, our method can inpaint the sparse point cloud into a dense radiance field with a photorealistic appearance. Please refer to the supplemental videos for a free-view rendering of the generated avatars and their corresponding point cloud.



Figure 8. Rendering of more hairstyles from the training set.



Figure 9. **Rendering of more hairstyles from the test set.**



Figure 10. **Visualization of the sparse point clouds for more hairstyles from the training set.**



Figure 11. Visualization of the sparse point clouds for more hairstyles from the test set.